# Some *ab initio* thoughts on the bonding in O$_3$H

## Apostolos Kalemos

Taylor & Francis
Taylor & Francis Group

Check for updates

RESEARCH ARTICLE

# Some *ab initio* thoughts on the bonding in O₃H

Apostolos Kalemos 

Department of Chemistry, Laboratory of Physical Chemistry, National and Kapodistrian University of Athens, Athens, Hellas

**ABSTRACT**
We study the ground $\tilde{X}^2A''$ state of O₃H ( = $O_aO_bO_cH$) with single (RCCSD(T)) and multi (MRCI) reference correlation methods in order to shed some light on its bonding mechanism in connection with its low dissociation energy and rather long bond distance ($O_aO_b - O_cH$). For such a task all three dissociation/formation paths were considered ($O_2 + OH$, $O + O_2H$, and $O_3 + H$) and the associated nonadiabatic coupling matrix elements were examined. It appears that the excited states of the above asymptotic fragments participate in the equilibrium wavefunction of O₃H in a way that results in a symmetry broken structure.
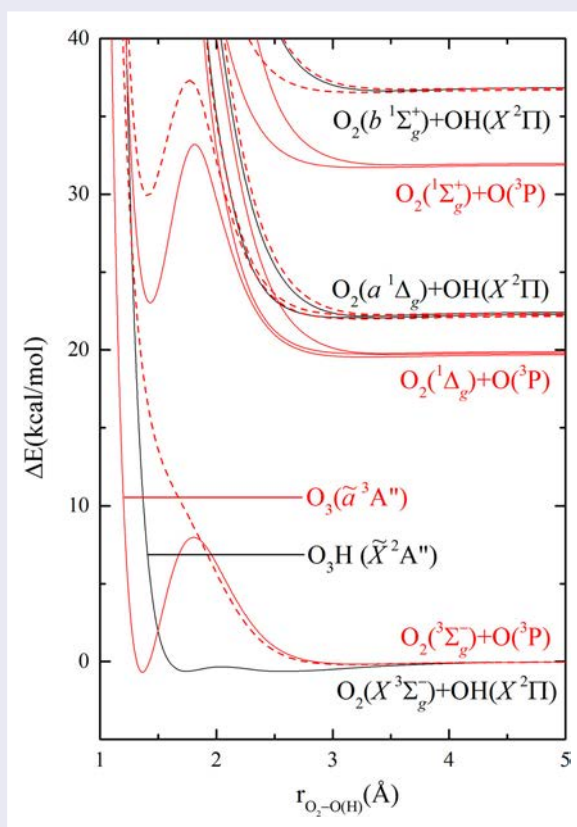
## 1. Introduction

The hydridotrioxygen (O₃H = $O_aO_bO_cH$) radical is a fascinating molecular species that has received considerable experimental and theoretical attention due to its atmospheric importance and purely academic interest; see e.g. Refs. [1–10] and references therein for a detailed

**CONTACT** Apostolos Kalemos ✉ kalemos@chem.uoa.gr 🖃 Department of Chemistry, Laboratory of Physical Chemistry, National and Kapodistrian University of Athens, Panepistimiopolis, Athens 157 71, Hellas

This article has been corrected with minor changes. These changes do not impact the academic content of the article.

historical account. From a purely academic point of view the intricate features of its chemical bonding and geometric equilibrium parameters nurtured a cease-less quest to unravel these mysteries; see e.g. Ref. [1]. In particular, the unexpectedly long $O_bO_c$ bond, $r_0(exp) = 1.688$ Å [11] and the surprisingly low dissociation energy $(O_aO_b - O_cH)$, $D_0(exp) = 2.93 \pm 0.07$ kcal/mol [12] seek for rationalisation. The purpose of this computational study is therefore to illuminate all these interesting questions.

## 2. The $O_3H$ saga

It is quite tempting and thought provoking to start thinking on this species by considering its equilibrium structure (for our purposes the most stable trans-isomer will be considered throughout the current study, the analysis provided holds true for the cis-isomer as well). We will rely on the results suggested by Bartlett *et al.* [7] of semi experimental character shown in Scheme 1.

These geometrical features trigger the following comments and thoughts. The $r(O_aO_b) = 1.215$ Å is practically identical to the equilibrium distance of $O_2$ in its first exci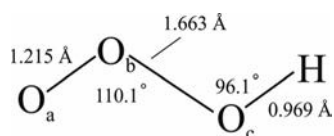ted $a^1\Delta_g$ state $(T_e(exp) = 7918.1$ cm$^{-1} = 0.982$ eV and $r_e(exp) = 1.2156_3$ Å) [13] and this implies that the $O_2$ $(= O_aO_b)$ moiety is *in situ* found in this particular excited state. This was only lately recognised [8] on the basis of nonadiabatic coupling matrix elements (NACME) between the first two adiabatic potential energy profiles (PEP) of $^2A''$ symmetry correlating to $O_2$ $(X^3\Sigma_g^-) + OH(X^2\Pi)$ and $O_2$ $(a^1\Delta_g) + OH(X^2\Pi)$, respectively (see Figure 1 for current results).

As strange as it may sound this is also the case in the simpler but similar $O_2H$ species. Its ground $\tilde{X}^2A''$ state relates diabatically to $O_2$ $(a^1\Delta_g)$ although its adiabatic end product is clearly $O_2$ $(X^3\Sigma_g^-)$ (see Figure 2). We can certainly ask why $O_2$ gets excited to $a^1\Delta_g$ upon interaction with either H ($^2S$) or OH ($X^2\Pi$) and does not remain in its ground $X^3\Sigma_g^-$ state?

A rationalisation may be given by the GVB results of the ground $O_2$ $(= O_aO_b)$ state [14] that predict one $\sigma$ bond $(2p_z(O_a)–2p_z(O_b))$, two $\pi$ bonds through the complete delocalisation of the $2p_x^2(O_a)$ and $2p_y^2(O_b)$ electron pairs towards $O_b$ and $O_a$, respectively, and two one electron [15] $\pi$ bonds through the



**Figure 1.** NACMEs between the first four $O_3H$ ($^2A''$) states along the $O_2 + OH$ dissociation path at the MRCI/cc−pVTZ computational level. The arrow in both curves point to the barrier's height. The geometry of the molecular fragments is at the equilibrium structure of $O_3H$.

complete delocalisation of the $2p_y^1(O_a)$ and $2p_x^1(O_b)$ electrons towards $O_b$ and $O_a$, respectively. The delocalisation energy amounts to $\sim 100$ kcal/mol [16] or even more [17] and it seems that this is the reason for its chemical inertness. This stabilisation energy is diminished by 0.982 eV $(= T_e(a^1\Delta_g \leftarrow X^3\Sigma_g^-))$ in $a^1\Delta_g$ whose $A_2(C_{2v})$ component share the same electronic distribution with the ground $X^3\Sigma_g^-$ state disregarding their different spin symmetry. The addition of H to $O_2$ in order to form $O_2H$ $(\tilde{X}^2A'')$ localises its $\pi(a')$ electrons and reduces rather significantly the delocalisation of its $\pi(a'')$ electrons [18]. As a consequence of this electronic rearrangement the OO bond is now $r_e(O - OH) = 1.335$ Å (RCCSD(T)/cc–pVTZ, see Table 1 and experimental value [19]) versus $1.2156_3$ Å $(= r_e(a^1\Delta_g))$ [13] while the O–O bond strength is $D_e(O–OH) = 63.2$ kcal/mol (RCCSD(T)/cc–pVTZ) as compared to the experimental value of $D_e(O_2$ in $a^1\Delta_g) = D_e(X^3\Sigma_g^-) - T_e(a^1\Delta_g) = 117.96$ kcal/mol – 22.65 kcal/mol = 95.33 kcal/mol [13]. The addition of a second H atom to form HOOH $(\tilde{X}^1A')$ further enhances



**Scheme 1.** Equilibrium molecular parameters of trans-$O_3H$ $(\tilde{X}^2A'')$ of semi experimental character; see Ref. [7] for details.
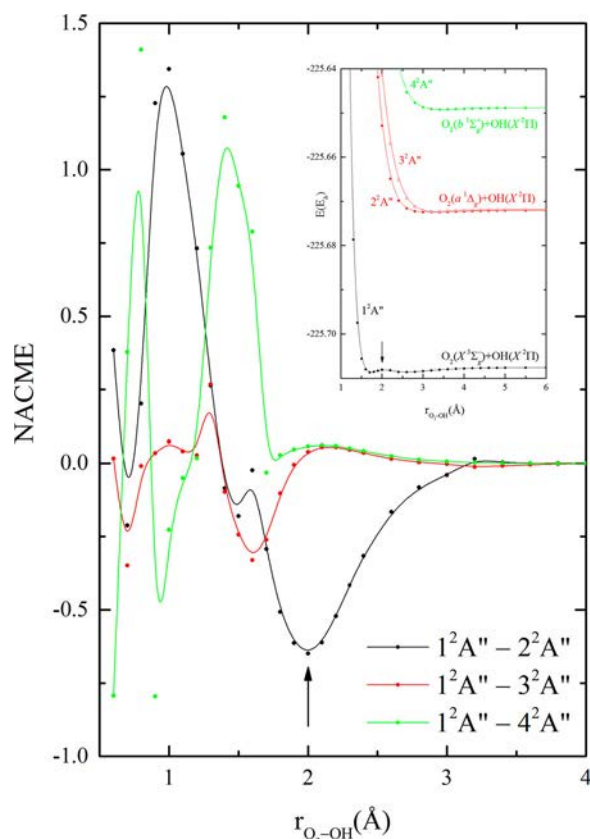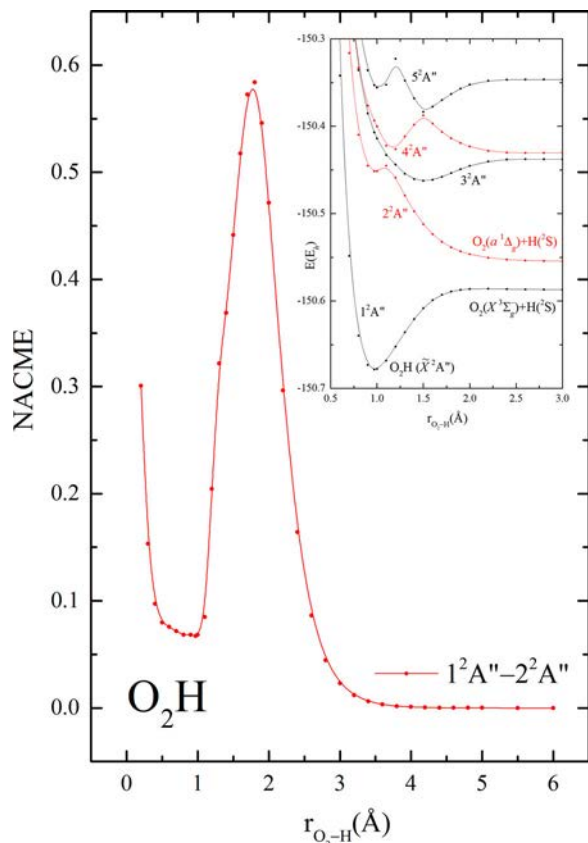
**Figure 2.** NACME between the first two $O_2H$ ($^2A''$) states along the $O_2 + H$ dissociation path at the MRCI/cc−pVTZ computational level.

this electronic rearrangement, the OO bond length is $r_e = 1.458$ Å (RCCSD(T)/cc−pVTZ; see Table 1) and its binding energy is $D_e(\text{HO−OH}) = 52.4$ kcal/mol (RCCSD(T)/cc−pVTZ). The upshot of the above discussion is that the stabilisation energy in $O_2$ ($X^3\Sigma_g^-$) is too high to be 'spoiled' by addition reactions that proceed rather easier through its first excited $a^1\Delta_g$ state.

If we now consider that $O_3H(\tilde{X}^2A'')$ results from the reaction $O_3(\tilde{a}^3A''(^3A_2)) + H\ (^2S)$, then the *in situ* $O_3$ species is greatly distorted with respect to the $C_{2v}$ structure of the free $O_3$ molecule in its $\tilde{a}^3A''(^3A_2)$ state ($r_e = 1.341$ Å, $\theta_e = 98.8°$ at MRCI/cc−pVQZ, [20] see also the current results in Table 1). And this is highly unexpected and counterintuitive. It appears that the approach of an H atom triggers such an electronic rearrangement that results in a symmetry broken structure (SB) which is not the case for instance in $O_3^-$, a system isoelectronic to $O_3H$ (see Table 1). The evident question is why this happens. Most interestingly, the addition of a second H atom to form $HO_3H$ ( ← $HO_3 + H$ or ← $H + O_3 + H$) retains the $C_{2v}$ skeleton of $O_3$ ($r_{OO} = 1.425$ Å at CCSD(T)−F12/cc−pVTZ − F12) [21]. This strange behaviour *vis à vis* the addition of one or two H atoms is certainly a puzzling question.

The last way to form $O_3H$ is through the $O + O_2H$ formation path. As already discussed, $O_2H$ ($\tilde{X}^2A''$) correlates diabatically to $O_2$ ($a^1\Delta_g$). The OO distance along the $O_2 \rightarrow O_2H \rightarrow HO_2H$ sequence varies as follows $1.2156_3$ Å ($a^1\Delta_g$; see Ref. [13]) → $1.335$ Å ($\tilde{X}^2A''$; see Table 1) → $1.458$ Å ($\tilde{X}^1A$; see Table 1). Upon addition of an $O_a$ atom to $O_bO_cH$ the $O_bO_c$ distance gets significantly longer ($1.695$ Å at MRCI/cc−pVTZ; see Table 1) that was once classified as a non-true covalent bond [1]. Certainly, this is strange since the addition of OH to $O_2H$ (to form $HO_3H = HO−O−OH$) does not lead to such spectacular bonding extravaganzas.

In this present work we shall try to illuminate all of the above 'unusual' chemical facts concerning the ground $O_3H$ state. To this end single (RCCSD(T)) and multi (MRCI) reference correlation methods, based on full valence (SA)CASSCF reference wavefunctions, coupled with the cc−pVTZ and (aug)−cc−pV5Z basis set [22] were employed as implemented in MOLPRO [23].

**Table 1.** Energies $E$ (hartree) and molecular parameters (bond distances in Å and bond angles in degrees) of the different species studied in the present work.

| Species | $-E$ | Molecular parameters | | | | |
|---|---|---|---|---|---|---|
| OH ($X^2\Pi$) | $75.637557^a$ | $0.971^a{}_{OH}$ | | | | |
| $O_2H$ ($\tilde{X}^2A'$) | $150.711906^a$ | $1.335^a{}_{OO}$ | $0.971^a{}_{OH}$ | $103.92^a{}_{\angle OOH}$ | | |
| | $150.682471^b$ | $1.341^b{}_{OO}$ | $0.971^b{}_{OH}$ | $103.54^b{}_{\angle OOH}$ | | |
| $HO_2H$ ($\tilde{X}^1A$) | $151.358611^a$ | $1.458^a{}_{OO}$ | $0.964^a{}_{OH}$ | $99.55^a{}_{\angle OOH}$ | $113.84^a{}_{\angle HOOH}$ | |
| $O_3H(\tilde{X}^2A')$ | $225.767698^a$ | $1.232^a{}_{O_aO_b}$ | $1.584^a{}_{O_bO_c}$ | $0.969^a{}_{O_cH}$ | $109.70^a{}_{\angle O_aO_bO_c}$ | $96.87^a{}_{\angle O_bO_cH}$ |
| | $225.710029^b$ | $1.220^b{}_{O_aO_b}$ | $1.695^b{}_{O_bO_c}$ | $0.968^b{}_{O_cH}$ | $110.49^b{}_{\angle O_aO_bO_c}$ | $95.03^b{}_{\angle O_bO_cH}$ |
| | $225.865647^c$ | $1.225^c{}_{O_aO_b}$ | $1.581^c{}_{O_bO_c}$ | $0.969^c{}_{O_cH}$ | $109.65^c{}_{\angle O_aO_bO_c}$ | $97.50^c{}_{\angle O_bO_cH}$ |
| $O_3(\tilde{X}^1A'(^1A_1))$ | $225.229589^c$ | $1.267^c{}_{OO}$ | $117.19^c{}_{\angle OOO}$ | | | |
| | $225.165703^d$ | $1.270^d{}_{OO}$ | $116.89^d{}_{\angle OOO}$ | | | |
| $O_3(\tilde{a}^3A''(^3A_2))$ | $225.180945^c$ | $1.330^c{}_{OO}$ | $97.93^c{}_{\angle OOO}$ | | | |
| | $225.116219^d$ | $1.340^d{}_{OO}$ | $98.79^d{}_{\angle OOO}$ | | | |
| $O_3^-(\tilde{X}^2B_1)$ | $225.306154^c$ | $1.345^c{}_{OO}$ | $115.05^c{}_{\angle OOO}$ | | | |
| | $225.216013^d$ | $1.350^d{}_{OO}$ | $115.34^d{}_{\angle OOO}$ | | | |

$^a$RCCSD(T)/cc−pVTZ; $^b$MRCI/cc−pVTZ; $^c$RCCSD(T)/aug−cc−pV5Z; $^d$MRCI/aug−cc−pV5Z.

## 3. Results and discussion

One way to understand the formation of the chemical bonds is to dissociate the molecule along its different chemical routes and conclude based on the form of the PEPs and their associated NACMEs. In our case there are three such formation paths which, in ascending energy order, are $O_2 + OH$, $O + O_2H$, and $O_3 + H$. Adiabatically trans-$O_3H$ ($\tilde{X}^2A''$) correlates to $O_2$ ($X^3\Sigma_g^-$) + OH ($X^2\Pi$), O ($^3P$) + $O_2H$ ($\tilde{X}^2A''$), and $O_3$ ($\tilde{a}^3A''(^3A_2)$) + H ($^2S$) but the excited states of the fragments play a major role in the bonding mechanism as we shall see below. It is clear enough though that its electronic wavefunction should be such that it describes all formation/dissociation routes evenly at all points of the pertinent configurational space and for this to happen all 'necessary' ingredients should be present.

The lowest adiabatic end asymptote of $O_3H(\tilde{X}^2A'')$ is $O_2(X^3\Sigma_g^-)$+OH($X^2\Pi$) that gives rise to only one surface of $^2A''$ symmetry. A cut along the $O_2$ + OH path that retains the equilibrium molecular parameters of $O_3H$ is shown in Figure 1. A closer look of this PEP (see Figure 3) reveals two minima of comparable strength at 2.6 and 1.7 bohr. At the longest one the wavefunction retains the characteristics of infinity with no genuine bond formed but at 1.7 bohr and after an energy barrier peaked at 2.0 bohr a new bond is formed between the spin defining electron of the OH ($X^2\Pi$) radical and the $\pi^*(a')$ electron of $O_2$ ($a^1\Delta_g$). This is clearly seen in the evolution of the NACMEs between the two lowest adiabatic $^2A''$ energy profiles correlating to $O_2(X^3\Sigma_g^-)$ + OH($X^2\Pi$) and $O_2(a^1\Delta_g)$ + OH($X^2\Pi$), respectively; see Figure 1. This new bond is visualised in the valence bond Lewis (vbL) diagram of Scheme 2.

When OH ($X^2\Pi$) approaches $O_2$, its $2p_\pi(a'')$ electron pair interacts unfavourably with the $a''$ density of $O_2$ [10,14]. This 'congested' electronic density may be an explanation for the rather long $O_bO_c$ (= 1.695 Å; see Table 1) bond distance. The adiabatic dissociation energy is found experimentally to be $D_0(exp) = 2.93 \pm 0.07$ kcal/mol [12] but the intrinsic (diabatic) binding energy is $D_0(exp) + T_e$ $(a^1\Delta_g \leftarrow X^3\Sigma_g^-)$ [13] = 25.6 kcal/mol. It is worth mentioning the fact that within $O_3H$ both $O_aO_b$ and $O_bO_c$ moieties are found *in situ* in their excited $a^1\Delta_g$ state while $O_aO_bO_c$ is found in a SB structure. The presence of an H atom breaks the symmetric environment of $O_3$ and it spoils the delocalisation of both in plane and out of plane electrons (see e.g. the form of some valence orbitals in Table 2). In a VB language this means that not all symmetry related resonant forms are present in the wavefunction that consequently leads to a SB structure; see e.g. Ref. [20].
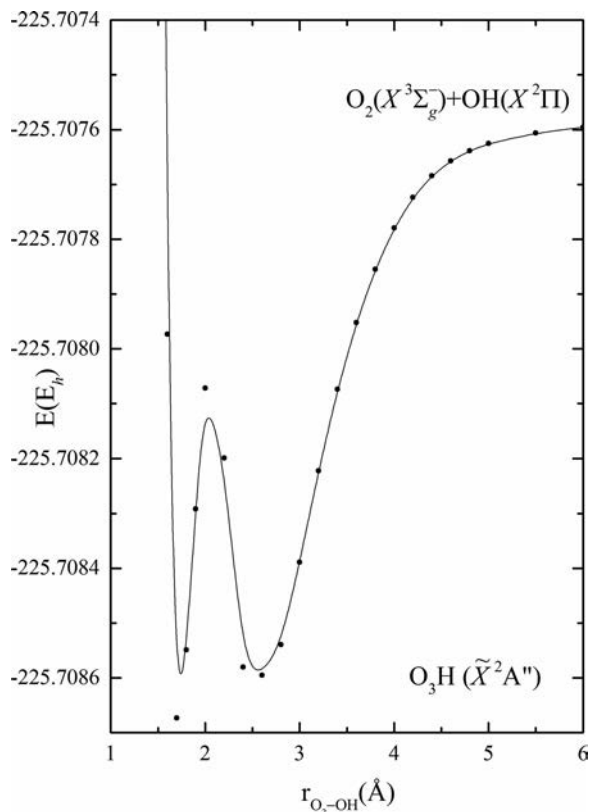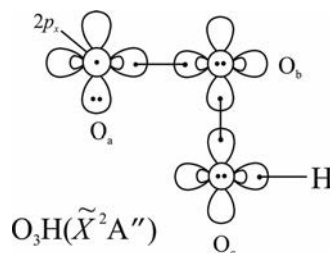


**Figure 3.** PEP of the ground $^2A''$ surface of $O_3H$ along the $O_2$ + OH dissociation path at the MRCI/cc−pVTZ computational level. The geometry of the molecular fragments is at the equilibrium structure of $O_3H$.



**Scheme 2.** vbL diagram depicting the ground $O_aO_bO_cH$ state.

Based on the vbL diagram of Scheme 2 it is tempting to consider the $O + O_2H$ formation path. The lowest adiabatic asymptote along this chemical route is $O(^3P) + O_2H$ ($\tilde{X}^2A''$) but as shown in Figure 4 it is initially repulsive due to its asymptotic electronic arrangement; see the vbL diagram of Scheme 3.

Instead, its diabatic end channel is O ($^3P$) + $O_2H$ ($1^2A'$) with an infinity electronic configuration as the one shown in Scheme 2. But as one can see in Figure 4 the PEP arising from O ($^1D$) + $O_2H$ ($\tilde{X}^2A''$) plummets vigorously affecting the lower PEPs. This is also corroborated by the large ($\sim 0.5$) value of the NACME of the associated PEPs.

**Table 2.** CASSCF molecular orbitals of $O_3$ ($\tilde{a}^3A''(^3A_2)$), of the distorted $O_3$ ($^{1,3}A''$; $r = 1.220$ and $1.695$ Å, $\theta = 110.49°$) moieties, and finally of $O_3H$ ($\tilde{X}^2A''$). The O atoms are represented by black spheres and the H atom by a white sphere.

| # MO | $O_3$ ($\tilde{a}^3A''$) | distorted $O_3(^1A'')$ | distorted $O_3(^3A'')$ | $O_3H$ ($\tilde{x}^2A''$) |
|---|---|---|---|---|
| $9a'$ | | | | |
| $10a'$ | | | | |
| $11a'$ | | | | |
| $1a''$ | | | | |
| $2a''$ | | | | |
| $3a''$ | | | | |

This means that the electronic arrangement reflecting the above end asymptote should be present in the wavefunction of the ground $O_3H$ state, and this is shown in the vbL diagram of Scheme 4.

Scheme 4 features a dative bond between $O_a$ ($\sim {}^1D$) and $O_bO_cH$ ($\tilde{X}^2A''$) with an overall electronic distribution similar to the one in the vbL diagram of Scheme 2.

Last but not least the $O_3 + H$ path, perhaps the most intriguing one since it leads to a dramatic structural reorganisation leading to a highly distorted SB structure of the *in situ* $O_3$ moiety. Adiabatically $O_3H$ ($\tilde{X}^2A''$) relates to $O_3$ ($\tilde{a}^3A''(^3A_2)$) that is the first excited A'' state of $O_3$. As already mentioned in Section 2 it is

highly surprising the fact that the addition of an H atom severely damages the symmetric nuclear framework of $O_3$ while this is not the case in the isoelectronic $O_3^-$ species or even in $HO_3H$. The latter species features the two H atoms above and below the $O_aO_bO_c$ plane at dihedral angles of $\sim 100°$ with an $O_aO_bO_c$ angle of $107.0°$ and OO distance of $1.425$ Å [21]. This implies two singly occupied $O_3$ $a''$ orbitals. The $O_3$ state with such characteristics is the first $^3A'$ one with an OO distance and OOO angle of $1.354$ ($1.355$) Å and $108.55$ ($108.47$)°, respectively, and separation energy of $T_e(^3A'(^3B_2) \leftarrow \tilde{X}^1A'(^1A_1)) = 11,063$ ($10,793$) cm$^{-1}$ at the MRCI(+Q)/cc − pVQZ computational level [20].
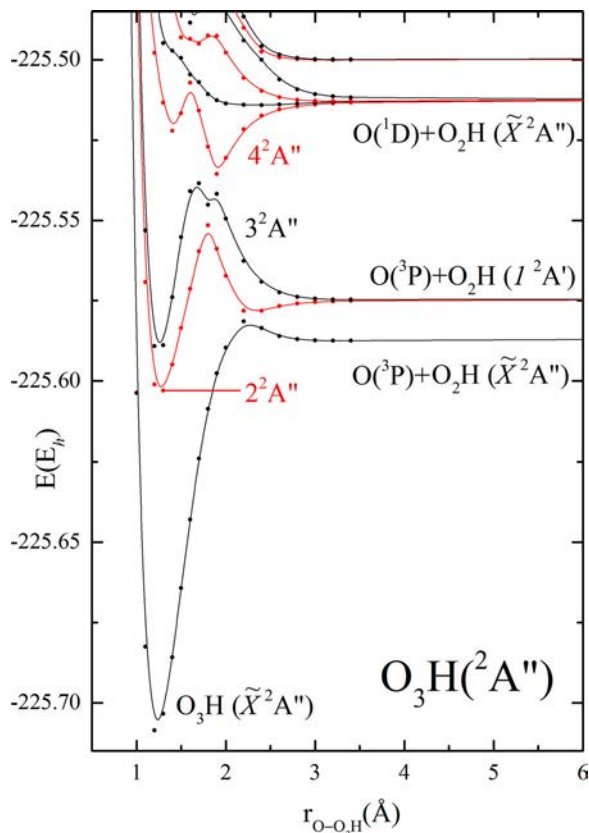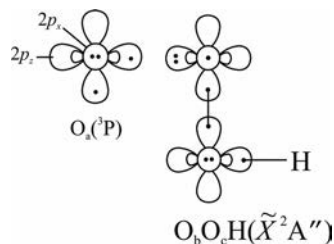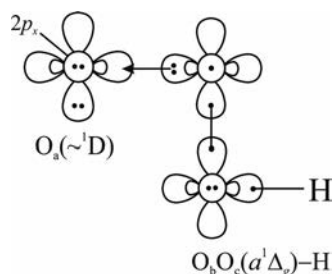
**Figure 4.** PEPs of $^2A''$ symmetry along the $O + O_2H$ dissociation path at the MRCI/cc−pVTZ computational level. The geometry of the molecular fragments is at the equilibrium structure of $O_3H$.



**Figure 5.** PEPs of $^3A''$ symmetry along the $O_2 + O$ dissociation path at the MRCI/cc−pVTZ computational level. In solid black curves $r(OO) = 1.348$ Å and $\theta = 98.61°$ and in dashed red curves $r(OO) = 1.220$ Å and $\theta = 110.48°$.



**Scheme 3.** vbL diagram depicting the repulsive $O_a$ $(^3P) + O_bO_cH$ $(\tilde{X}^2A'')$ interaction at infinity.



**Scheme 4.** vbL diagram depicting the attractive $O_a$ $(\sim {}^1D) + O_bO_cH$ $(\tilde{X}^2A'')$ interaction.

The addition of the two H atoms preserves the OOO angle and elongates the OO distance by roughly 0.075 Å due to the localisation of the two triplet coupled electrons. Interestingly, $HO_3H = (HO)-O-(OH)$ can be viewed as an OH substituted water (HOH) molecule.

In order to understand the SB structure emerging upon interaction with an H atom we should take a look at the electronic structure of $O_3$ $(\tilde{a}^3A''(^3A_2))$, of the distorted $O_3$ $(^3A''$; $r = 1.220$ and $1.695$ Å, $\theta = 110.49°$) moiety, and finally of $O_3H$ $(\tilde{X}^2A'')$. Their CASSCF equilibrium wavefunctions are $|\tilde{a}^3A''(^3A_2)\rangle \cong 0.89|(1-8)a'^2 9a'^2 10a'^1 1a''^2 2a''^2 3a''^1\rangle + 0.34|(1-8) a'^2 9a'^1 10a'^2 1a''^2 2a''^1 3a''^2\rangle, |^3A''\rangle \cong |(1-8)a'^2 9a'^1 (0.88 \times 10a'^2 - 0.31 \times 11a'^2)1a''^2 2a''^2 3a''^1\rangle$, and $|\tilde{X}^2A''\rangle \cong |(1-9)a'^2 (0.91 \times 10a'^2 - 0.29 \times 11a'^2)1a''^2 2a''^2 3a''^1\rangle$, respectively, while the pertinent orbitals are shown in Table 2. The electronic character of the distorted $O_3$ $(^3A'')$ moiety and the ground $O_3H$ species are practically the same. In the former species the $9a'$ orbital is localised on the incoming O atom while the $10a'$ and $11a'$ orbitals describe mainly the $O_aO_b-O_c$ bond in a GVB way. The same prevails in $O_3H$ in which case the $9a'$ orbital is now the $O_aO_bO_c-H$ bond. In order to understand the highly
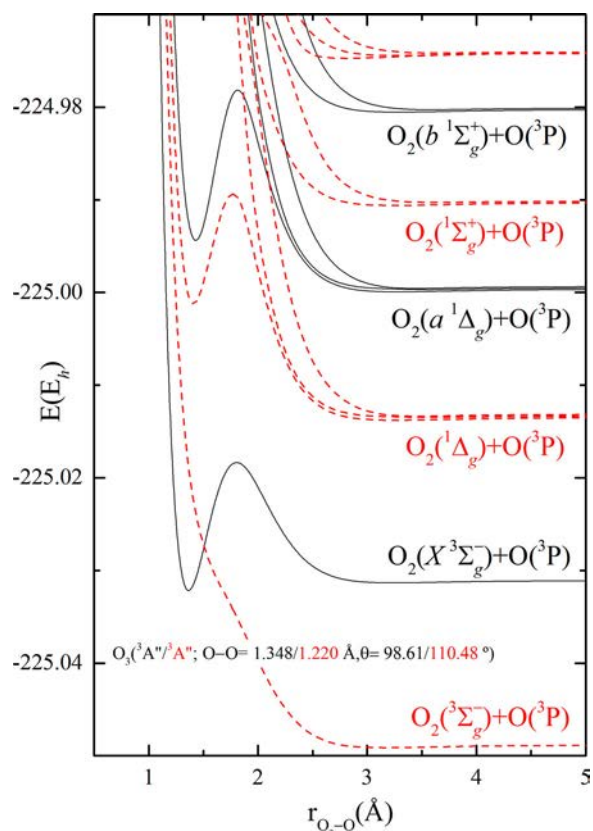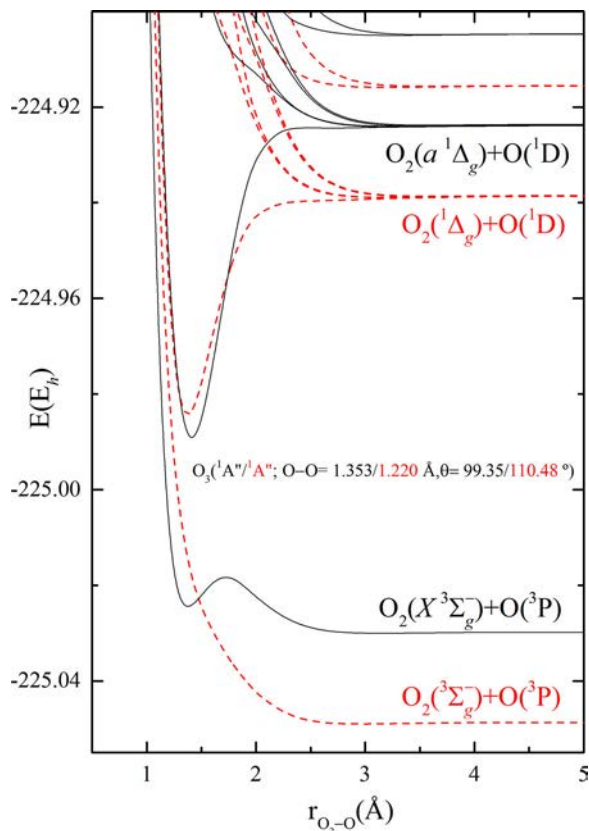
**Figure 6.** PEPs of $^1A''$ symmetry along the $O_2 + O$ dissociation path at the MRCI/cc−pVTZ computational level. In solid black curves $r(OO) = 1.353$ Å and $\theta = 99.35°$ and in dashed red curves $r(OO) = 1.220$ Å and $\theta = 110.48°$.
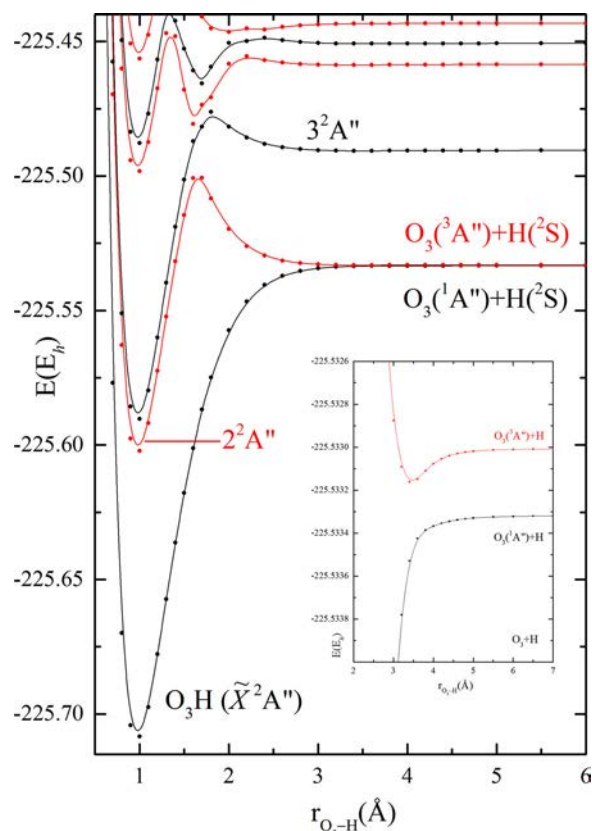


**Figure 7.** PEPs of $^2A''$ symmetry along the $O_3 + H$ dissociation path at the MRCI/cc−pVTZ computational level. The geometry of the molecular fragments is at the equilibrium structure of $O_3H$.

distorted $O_3$ moiety inside $O_3H$ we should examine the $O_aO_b + O_c$ interaction of both $^3A''$ and $^1A''$ symmetry. This is shown in Figures 5 and 6 where several PEPs are contrasted for $O_aO_b$ distances of 1.348 Å (OO distance in $O_3$ ($\tilde{a}^3A''(^3A_2)$) at MRCI/cc − pVTZ) / 1.220 Å ($O_aO_b$ distance in $O_3H$ ($\tilde{X}^2A''$)) and 1.353 Å (OO distance in $O_3$ ($^1A''(^1A_2)$) at MRCI/cc − pVTZ) / 1.220 Å ($O_aO_b$ distance in $O_3H$ ($\tilde{X}^2A''$)), respectively. As one can see, the topology of the PEPs changes dramatically when H approaches diabatically the distorted $O_3$ fragment in its $^1A''$ symmetry (see the inset of Figure 7), a fact rather unexpectedly. It is interesting to examine the evolution of the PEPs along the $O_2 + O(H)$ interaction route depicted in Figures 5–7 since this will address the puzzle of the distorted geometry in $O_3H$. As one can see in Figure 5 the $O_3$ $\tilde{a}^3A''(^3A_2)$ minimum lays on the lowest (lowest solid black curve) adiabatic energy surface dissociating to $O_2$ $(X^3\Sigma_g^-) + O$ $(^3P)$ after an energy barrier is surpassed. At the distorted $O_3$ geometry (when the $O_aO_b$ distance is 1.220 Å) this $^3A''$ minimum does not exist (see the lowest red dashed curve in Figure 5). The same situation prevails in the $^1A''$ symmetry (see Figure 6). At the distorted $O_3$ geometry, i.e. $O_aO_b = 1.220$ Å and $O_bO_c = 1.695$ Å,

the $^1A''$ symmetry is slightly lower than the $^3A''$ one ($E(^1A'') = −225.034\,42$ $E_h$ and $E(^3A'') = −225.033\,68$ $E_h$ at the MRCI/cc–pVTZ level) and that means that both $^1A''$ and $^3A''$ symmetries interact strongly with the approaching H atom (see the inset of Figure 7). It is worth saying at this point that the $^1A''$ minimum correlates to $O_2$ $(a^1\Delta_g) + O$ $(^1D)$ (see Figure 6). The rather long $O_bO_c$ ($= 1.695$ Å) distance can be rationalised based on the topology of the PEPs. The potential minima of both $^{1,3}A''$ symmetries appear at $\sim 1.4$ Å, thus an H atom binds to an $O_3$ moiety at no less than this bond distance. Additionally, as long as the $O_cH$ bond is formed, the $O_aO_b$ one is weakened and consequently it becomes longer.

A final comment concerning the similarity of the profiles of the $O_2 + O$ and $O_2 + OH$ interactions is in order (see Figure 8). An O atom, due to its spherical symmetry, offers three ways of attack ($^3P$, $M_L = 0(xy)$, $\pm 1(xz, yz)$) while the OH radical, due to its cylindrical symmetry, ($X^2\Pi$, $\Lambda = \pm 1$) only two. This explains the reduced number of the PEPs of $^3A''$ symmetry connected adiabatically with the three lowest asymptotic channels, i.e. $O_2$ $((X)^3\Sigma_g^-$, $(a)^1\Delta_g$, $(b)^1\Sigma_g^+) + O$ $(^3P)$ (or OH $(X^2\Pi)$). Moreover, it is interesting to consider the change of the
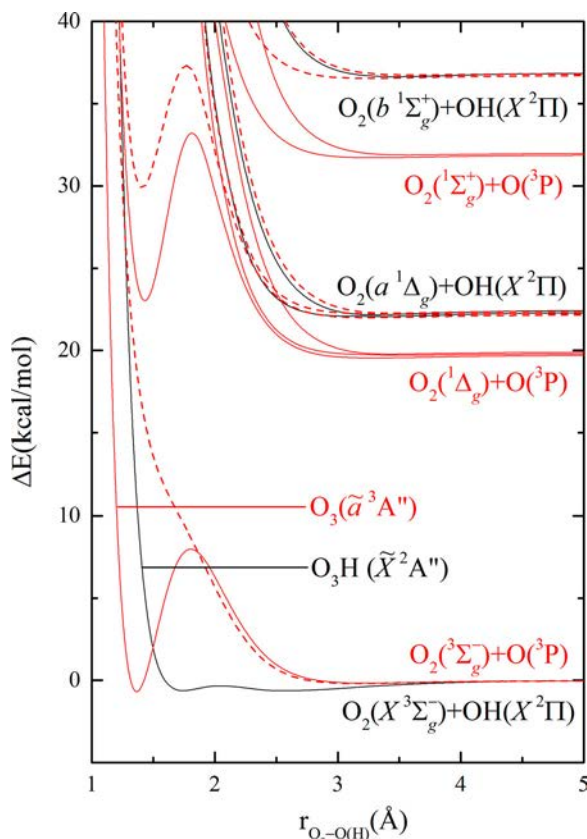
**Figure 8.** PEPs along the $O_2 + O$ (red curves) and $O_2 + OH$ (solid black curve) dissociation paths at the MRCI/cc−pVTZ computational level. The zero of energy is at the respective ground state fragments.

$O_3$ ($\tilde{a}^3 A''(^3A_2)$) and $O_3H$ ($\tilde{X}^2 A''$) PEPs. The rather high potential barrier that gives rise to a bound $O_3$ species (lowest solid red curve in Figure 8) is smoothened to a 'calm' $O_3H$ curve (solid black curve) that qualitatively shares the same features (see also Figure 3) and all that through the intermediate of a repulsive curve (dashed red curve) that implies the participation of excited states via avoided crossings.

## 4. Conclusions

We have studied the ground $\tilde{X}^2 A''$ $O_3H$ state through both single (RCCSD(T)) and multi (MRCI) reference methods along its three dissociation/formation paths that in ascending energy order are $O_2 + OH$, $O + O_2H$, and $O_3 + H$. The purpose of such a comparative study is to shed some light on the peculiar features of the species, namely its low dissociation binding energy ($O_aO_b−O_cH$) and the rather long bond length between the two middle oxygen atoms. The presence of the H atom, i.e. the fact that an in plane $O_3$ electron localises to a particular O ($= O_c$) atom in order to get coupled with H, results in a SB structure since the delocalisation of the in and out

of plane $O_3$ electrons is hindered. This is not the case in HO−O−OH (HO$_3$H) since the H atoms bind quasi perpendicularly to two triplet coupled $a''$ $O_3$ electrons. The low dissociation energy is rationalised through the participation of excited fragment states (see e.g. Figure 8) while the long $O_bO_c$ distance can be explained with the help of the topology of the $O_2 + O$ interaction (see Figures 5 and 6).

## Disclosure statement

No potential conflict of interest was reported by the authors.

## ORCID

*Apostolos Kalemos* http://orcid.org/0000-0002-1022-0029

## References

[1] A. Mansergas, J.M. Anglada, S. Olivella, M.F. Ruiz-López, and M. Martins-Costa, Phys. Chem. Chem. Phys. **9**, 5865–5873 (2007). doi:10.1039/b711464h
[2] J.M. Anglada, S. Olivella, and A. Solé, J. Chem. Theor. Comp. **6**, 2743–2750 (2010). doi:10.1021/ct100358e
[3] A.J.C. Varandas, Phys. Chem. Chem. Phys. **13**, 9796–9811 (2011). doi:10.1039/c1cp20221a
[4] A.J.C. Varandas, Phys. Chem. Chem. Phys. **13**, 15619–15623 (2011). doi:10.1039/c1cp20791a
[5] A.J.C. Varandas, J. Chem. Theor. Comp. **8**, 428–441 (2012). doi:10.1021/ct200773b
[6] A.J.C. Varandas, Int. J. Quantum Chem. **114**, 1327–1349 (2014). doi:10.1002/qua.24580
[7] M.A. Bartlett, A.H. Kazez, H.F. Schaefer, and W.D. Allen, J. Chem. Phys. **151** (1–23), 094304 (2019). doi:10.1063/1.5110291
[8] X. Hu, J. Zuo, C. Xie, R. Dawes, H. Guo, and D. Xie., Phys. Chem. Chem. Phys. **21**, 13766–13775 (2019). doi:10.1039/C9CP02206F
[9] T. Trabelsi and J.S. Francisco, J. Chem. Phys. **152** (1–8), 064304 (2020). doi:10.1063/1.5134838
[10] B.A. Lindquist, T.Y. Takeshita, and T.H. Dunning Jr, J. Phys. Chem. A **120**, 2720–2726 (2016). doi:10.1021/acs.jpca.6b02014
[11] K. Suma, Y. Sumiyoshi, and Y. Endo, Science. **308**, 1885–1886 (2005). doi:10.1126/science.1112233
[12] S.D. Le Picard, M. Tizniti, A. Canosa, I.R. Sims, and I.W.M. Smith, Science. **328**, 1258–1262 (2010). doi:10.1126/science.1184459
[13] 'Constants of Diatomic Molecules' by K.P. Huber and G. Herzberg (data prepared by J.W. Gallagher and R.D. Johnson, III) in NIST Chemistry WebBook, NIST Standard Reference Database Number 69, Eds. P.J. Linstrom and W.G. Mallard, National Institute of Standards and Technology, Gaithersburg MD, 20899, doi:10.18434/T4D303.
[14] B.J. Moss, F.W. Bobrowicz, and W.A. Goddard III, J. Chem. Phys. **63**, 4632–4639 (1975). doi:10.1063/1.431248
[15] D.W.O. de Sousa and M.A.C. Nascimento., Phys. Chem. Chem. Phys. **21**, 13319–13336 (2019). doi:10.1039/C9CP02209K

[16] W.T. Borden, R. Hoffmann, T. Stuyver, and B. Chen, J. Am. Chem. Soc. **139**, 9010–9018 (2017). doi:10.1021/jacs.7b04232

[17] D. Danovich, C. Foroutan-Nejad, P.C. Hiberty, and S. Shaik, J. Phys. Chem. A. **122**, 1873–1885 (2018). doi:10.1021/acs.jpca.7b11919

[18] T.H. Dunning Jr, S.P. Walch, and M.M. Goodgame, J. Chem. Phys. **74**, 3482–3488 (1981). doi:10.1063/1.441501

[19] Y. Beers and C.J. Howard, J. Chem. Phys. **64**, 1541–1543 (1976). doi:10.1063/1.432375

[20] A. Kalemos and A. Mavridis, J. Chem. Phys. 129, 054312 (1–8) (2008). doi:10.1063/1.2960629

[21] D.S. Hollman and H.F. Schaefer III, J. Chem. Phys. **136** (1–9), 084302 (2012). doi:10.1063/1.3684231

[22] T.H. Dunning Jr, J. Chem. Phys. **90**, 1007–1023 (1989). doi:10.1063/1.456153

[23] MOLPRO is a package of *ab initio* programs written by H.-J. Werner, P.J. Knowles, G. Knizia, F. R. Manby, M. Schütz, P. Celani, W. Györffy, D. Kats, T. Korona, R. Lindh, A. Mitrushenkov, G. Rauhut, K.R. Shamasundar, T.B. Adler, R.D. Amos, A. Bernhardsson, A. Berning, D.L. Cooper, M.J. O. Deegan, A.J. Dobbyn, F. Eckert, E. Goll, C. Hampel, A. Hesselmann, G. Hetzer, T. Hrenar, G. Jansen, C. Köppl, Y. Liu, A.W. Lloyd, R.A. Mata, A.J. May, S.J. McNicholas, W. Meyer, M.E. Mura, A. Nicklaß, D.P. O'Neill, P. Palmieri, D. Peng, K. Pflüger, R. Pitzer, M. Reiher, T. Shiozaki, H. Stoll, A.J. Stone, R. Tarroni, T. Thorsteinsson, and M. Wang. *MOLPRO, version 2012.1, a package of ab initio programs*; University College Cardiff Consultants Limited: Cardiff, U.K., 2008.